RSC Advances

ROYAL SOCIETY OF CHEMISTRY

www.rsc.org/advances

Journal Name

RSCPublishing

ARTICLE

Effect of the silicon carbide nanoparticles introduction on biological properties of porous polymer coatings

Cite this: DOI: 10.1039/x0xx00000x

Received 00th January 2012,
Accepted 00th January 2012

DOI: 10.1039/x0xx00000x

www.rsc.org/

A. Mzyk[a], R. Major[a], J. M. Lackner[b], F. Bruckert[c], P.Wilczek[d] and B. Major[a]

The multilayer polyelectrolyte films (PEMs) seem to be promising coatings to simulate the structure and behavior of the extracellular matrix. PEMs constructed through Layer by Layer deposition of oppositely charged polymers have become a powerful tool for tailoring biointerfaces. Films consist of chitosan/chondroitin sulfate polymers exhibit a fast biodegradability in the environment of human tissues. Lifetime extension of this material type could be implemented by its structure stabilization through the cross-linking or introduction of nanoparticles. Transmission electron microscopy (TEM) and high resolution transmission electron microscopy (HRTEM) methods were used to determine the microstructure and localization of the silicon carbide nanoparticles introduced to the extracellular like structure of the polymer coatings. The numerical analysis of nanoparticles dispersion and mechanical properties was verified by indentation measurements. Modified coatings biocompatibility was analyzed in cytotoxicity assay and microscopic observations of endothelial cells growth on the material surface. Comparison of stabilization methods including chemical cross-linking and SiC nanoparticles introduction into multilayer polyelectrolyte films has shown that both of stabilizers could be useful for biomedical applications. However, SiC nanoparticles application could be limited by slightly lower endothelialization efficiency and risk of cytotoxicity due to their release from coatings.

Keywords: Polyelectrolyte Multilayer Films, Silicon carbide, Nanoparticles, Cytotoxicity, Endothelialization

1. Introduction

The multilayer polyelectrolyte films (PEMs) seem to be promising coatings to simulate the structure and behavior of the extracellular matrix [1, 2]. PEMs constructed through Layer by Layer deposition of oppositely charged polymers have become a powerful tool for tailoring biointerfaces [3]. They are interesting for biomedical applications as thin coatings on artificial cardiovascular prostheses or as coverage of biosensor electrodes. The attention has been paid to chitosan (Chi) as a potential polysaccharide resource due to its brilliant properties, including biocompatibility, biodegradability, haemostatic activity, antibacterial properties, low cost and ability to accelerate wound healing [4]. Chondroitin sulfate (CS) is a natural extracellular matrix biopolymer with anti-inflammatory properties [5]. Sulfated glycosaminoglycans like CS possess binding affinity to growth factors and support their bioactivity [6]. Enhanced bioactivity can be imposed onto biomimetic PEM films by incorporating sensitive biomolecules, e.g. growth factors or enzymes [7]. Films consist of chitosan/chondroitin sulfate polymers exhibit a fast biodegradability in the environment of human tissues. Lifetime extension of this material type could be implemented by its structure stabilization through the chemical cross-linking or introduction of nanoparticles. Moreover, it is possible to control mechanical properties and make coatings more functional [8-10]. Recent research has been aimed at exploiting nanoparticles in polymeric network architectures [11, 12]. Products prepared by these approaches are leading to new composite systems [13, 14]. The optic transparency, easy deposition and quantitative response character of polyelectrolyte multilayer enhance the applicability of nanoparticle array based nanosensors in chemical and biological sensing [15, 16]. Among different kinds of nanomaterials, silicon carbide (SiC) which is a wide band gap semiconductor, has a range of properties, which makes it suitable for designing and improving sensing devices [17]. So far SiC nanoparticles have been used for determination of purine and pyrimidine DNA bases and electrochemical detection of nitric oxide [18, 19]. In this study we demonstrated for the first time to our knowledge, the effect of the silicon carbide nanoparticles introduction on mechanical and biological properties of the Chi/CS porous polymer coatings. The biological verification considered coatings cytotoxicity and endothelialization. We described the relation between cross-linking and nanoparticles immobilization influence on film's properties, in order to obtain fundamental information about nanoparticles - biopolymer interactions. Comparison of the both stabilization methods efficiency was a key point of investigations.

2. Materials and methods

The polyelectrolyte coatings were made from the cationic chitosan (Chi) and the anionic chondroitin sulfate (CS) purchased from Sigma-Aldrich. The low weight Chi and CS were applied. Chemicals for cross-linking i.e. 1-ethyl-3-(3-dimethylamino-propyl)carbodiimide (EDC), N-hydrosulfosuccinimide (NHS) were also supplied from Sigma-Aldrich. Human Umbilical Vein Endotheliala Cells were bought from Lonza Group Ltd. Cellular response was assessed based on application of Alexa Fluor®488 Phalloidin and DAPI supplied from Invitrogen. Cytotoxicity was assessed by staining with propidium iodide purchased from Sigma Aldrich.

2.1. Polyelectrolyte multilayer films manufacturing and chemical cross-linking

Polyelectrolyte multilayered films (PEMs) were deposited with a "layer-by-layer" technique onto 1.5 cm x 1.0 cm glass substrate material for mechanical and biological analysis or the silicon wafer for SEM/TEM observations. Substrates were activated by 10 M NaOH and washed with pure Milli-Q water. In order to obtain Chi solution, pre-dissolution step in acetic acid (0.1 M) was required. The CS polymer is well soluble in water, therefore pre-dissolution step was unnecessary. Finally, Chi and CS were prepared in 400 mM HEPES/0.15 M NaCl solution of pH 7.4 with concentration of 0.5 mg/ml and 1 mg/ml, respectively. Films were manufactured with an automatic dipping machine by an alternately immersing substrate in solutions of Chi and CS for 8 min each. After each deposition step, the substrate was rinsed in 0.15 M NaCl solution buffered at pH 7.4 to remove excess polyelectrolyte. The process was repeated until the desired number of 48 bilayers was obtained. Multilayer films were further processed for a cross-linking in order to stabilize the porous layers. The other group of the samples was left in a non-cross-linked state. The reason to preparation cross-linked and non-cross-linked materials was to prolong durability of the coatings and to analyze the effects on cell-material interactions. In order to perform chemical cross-linking process the 260 mM 1-ethyl-3-(3-dimethylaminopropyl)carbodiimide (EDC) and 100 mM N-hydroxysulphosuccinimide (NHS) was applied according to the protocol described elsewhere [20]. Reagents were prepared in 0.15 M NaCl solution buffered at pH 5.5 and mixed together in 1:1 volume ratio immediately before application. Polyelectrolyte films were incubated in EDC/NHS for 18 hours at 4^{o}C. Then the cross-linker solution was removed, and films were rinsed several times with 400 mM HEPES/0.15 M NaCl solution buffered at pH 7.4 to wash out non-reacted amounts of reagents. Washing procedure which is significant for exact cytotoxicity investigations was performed in two steps. Initially the coatings have been rinsing two times for one hour under slow shaking at room temperature each time. In the second step the coatings were conducted to three short (10 minutes each one) washes to have sureness that all of non-bonded cross-linker residues were removed

2.2. Nanoparticles introduction

SiC nanoparticles were introduced to cross-linked and non-cross-linked films by the plasma assisted chemical vapour deposition (PACVD) [21]. The deposition was 5 s lasting process. Before nanoparticles introduction substrates were dried and introduced into the vacuum chamber. The chamber was pumped to reach the vacuum down to 5 Pa. SiC nanoparticles were grown in hexamethyldisiloxane (HMDSO, Sigma Aldrich) atmosphere of 20 Pa pressure. The nanoparticles were achieved at 32^{o}C with less than 2^{o}C heating during deposition in plasma. In order to obtain better incorporation rate in PEMs, the kinetic energy of deposited SiC nanoparticles has been reduced by introducing an inert gas (argon) into the reaction chamber during the PACVD process. The average number of single SiC nanoparticles per 100 nm^2 surface was calculated based on high resolution transmission electron microscopy (HRTEM) images.

2.3. Topography and microstructure analysis

Topography observations were done using Scanning Electron Microscopy technique (SEM) on Quanta 200 3D. Microstructure characterization was performed using Transmission Electron Microscopy technique (TEM), on sample cross-section. The Tecnai G2 F20 (200 kV) FEG was used for analysis. Thin foils for TEM observations were prepared directly from the place of interest using focused ion beam technique (equipped with in situ micromanipulator). The Quanta 200 3D DualBeam was used for FIB preparation [22]. Observations were performed in a bright field mode.

2.4. Nanoparticles dispersion numerical analysis

Numerical analysis was performed using the finite element method using ADINA program System v8.7. Axisymmetric model has been adopted. Discretisation was carried out using an axis symmetric component 2D SOLID. Mesh density on the thickness of the ellipse was 2 elements, and mesh density on the circuit of the ellipse 10 items. The 100 time steps were applied. For unload 50 time steps were used. For the study a single geometry of the ellipse with the following parameters was applied: the length of the horizontal half-axis of the ellipse = 1000 [nm], the length of the vertical half-axis of the ellipse = 100 [nm], thickness of the ellipse = 140 [nm]. Three materials were used in the numerical model, polymer layer with nanoparticles, pure polymer layer and glass substrate. In all cases an elastic – plastic model of the material was applied. Using numerical analysis, nanoindentation test was simulated. The nanoindentation is one of the most common tests used to evaluate the mechanical properties at the nanoscale. The radius of the nanoindenter ball was 500 nm. Ball ended cone angle was equal to 140°6'. The adopted model allowed to including the elastic and permanent deformation of the material, which occurred in the porous layer and the substrate. In each of the modelled ellipse the contact surfaces on the free surfaces were assumed, both inside and outside of the ellipse. The contact surfaces allowed to taking into account the porosity of these materials. The adopted numerical analysis was simplified in relation to reality. It allows qualitatively evaluate the phenomena occurring during the deformation of the porous polyelectrolyte multilayer as well as the polymer film modified by nanoparticles.

2.5. Experimental verification of coating's mechanical properties

Simulated mechanical properties were verified in experimental approach. Indentation tests were performed at 10mN load using the Berkovich indenter. The loading and unloading speed was 20 mN/min. The holding time at a maximum load was extended to 30s. Prolonged time allowed for elimination of the polymer coating viscoelastic (creep) behaviour influence on preformed measurements. Measurements were carried out in ten places on each sample. A statistical analysis (two-way ANOVA and Tukey post hoc test, P value smaller than 0.05 was considered as significant – Statistica 10.0 PL) was performed on three replicates for all investigated specimens.

2.6. Cytotoxicity

Potential cytotoxic effect was determined according to the ISO 10993-5:2009 standards [23]. Samples in size of 1.5 cm^2 were placed in confluent mouse fibroblast (L929; ATCC) cultures (about 5 x 10^5 cells) and have been incubated for 48 hours at 37°C. Then cells were stained by propidium iodide (PI). Cultures incubated either with cross-linked, non-crosslinked and samples with/without nanoparticles were analyzed in comparison with control cultures. Images were taken with the Axio Observer Z1 inverted microscope equipped with a camera and quantified using AxioVision 4.6 software (Carl Zeiss MicroImaging). A statistical analysis (two-way ANOVA and Tukey post hoc test, P value smaller than 0.05 was considered as significant – Statistica 10.0 PL) was performed on three replicates from each treatment.

2.7. Coating's settlement by endothelial cells

HUVECs (Human Umbilical Vein Endothelial Cells) were seeded with density of $3x10^4$ cells/cm^2 and cultured on all analyzed variants of scaffolds (Table 1). The polystyrene was used as a control substrate. After 48 hours of incubation endothelial cells were fixed with 4% paraformaldehyde. For the cell - material interaction analysis, fluorescent methods were applied. The samples were stained with Alexa Fluor 488 phalloidin in order to visualize cytoskeleton structure and with DAPI to show cells' nucleus. Images were acquired using a confocal laser scanning microscopy (CLSM) Exciter5 AxioImiger. Data were processed with the CLSM Zen 2008 software. The morphology and differences in cell number were determined after 48 hours incubation on each surface. A statistical analysis was performed using the two-way ANOVA and the Tukey post-hoc test for the P value smaller than 0.05 considered as significant (Statistica 10.0 PL). Examination was carried out on three replicates from each treatment.

3. Results

3.1. Topography and microstructure analysis

The first attempt to the PACVD method of SiC nanoparticles introduction into polyelectrolyte multilayer coating was described in the recent paper. It reveals nanoparticles penetration through the polyelectrolyte coating and nucleation directly on the substrate. Only a small number of SiC was homogeneously distributed within the film [24]. Herein, the Scanning Electron Microscopy technique was also used to the top view analysis of coatings. Examination of the nanoparticles distribution has shown aggregate-like structure formation either in non-cross-linked and cross-linked polyelectrolyte films (Fig. 1). No significant differences between samples containing nanoparticles, except variable homogeneity in aggregates distribution related to PACVD protocol specificity were noticed. However, it was found that topography differs between cross-linked and non-cross-linked films (Fig. 2). Surface roughness decreased after Chi/CS polyelectrolyte multilayer cross-linking. Based on the Transmission Electron Microscopy (TEM) analysis, the immobilization of the nanoparticles in the polyelectrolyte coating was observed. TEM images did not indicate visible significant differences between microstructure of non-cross-linked and cross-linked samples containing SiC nanoparticles (Fig. 3). Similar observations were noticed for films without nanoparticles (Fig. 4). High Resolution Transmission Electron Microscopy (HRTEM) revealed the formation of three zones within polyelectrolyte multilayer, the SiC non-implanted zone, the highest density of SiC nanoparticles zone and the single SiC nanoparticles implanted zone (Fig. 5A). HRTEM images indicated the average size of nanoparticles in range of 1-5 nm and mean value of the 17 single particles per 100 nm^2 in the nanoparticles dense zone and 8 single particles per 100 nm^2 in the deeper coating layers, located closer to the substrate surface. Occurrence of the cubic 3C-SiC polytype of nanoparticles in the coating was confirmed by the HRTEM intermediate filtered images (Fig. 5B, C).

3.2. Nanoparticles dispersion numerical analysis

Porous multilayer structure was modelled in the form of elliptic elements with empty volumes (Fig. 6A). In the simulation nanoparticles were located in the nodes of arcs in the model of the coating (Fig. 6B). The geometry of the following parameters was applied to simulate mechanical properties of the porous structure with or without SiC nanoparticles. Adopted radius of the polyelectrolyte multilayer model was 3000 nm. During the numerical analysis the applied clearance between indenter and first layer before indentation was 98 nm. In contrast, the distance between the porous layer and the substrate before indentation was 1440 nm. Table 2 shows the applied loads. In order to determine the distribution of plastic strain in the numerical model both the substrate and the polyelectrolyte multilayer material was modelled as an elastic-plastic material. The points marked in red indicate the reinforcing nanoparticles incorporated in the coating. The coating with or without nanoparticles and the substrate mechanical properties introduced into the model are presented in Table 3. The distribution of plastic deformation occurring in the deformed porous material is shown in Figure 7. For time t = 100 s the deformation of the material under load F = 10 mN was observed. The results for t = 150 s, presents the deformation after removing the load. The value of plastic deformation for material with nanoparticles was 3.824 under loading, then after unloading was changed to 4.028.

3.3. Experimental verification of coating's mechanical properties

The performed studies on coatings' mechanical properties have shown that either cross-linking or SiC nanoparticles introduction into Chi/CS polyelectrolyte multilayer caused a significant increase in film stiffness (Fig. 8). The Young modulus value increased from 8.5 GPa for non-cross-linked samples to 10.3 GPa for 260 mM cross-linked films and to 72 GPa for non-cross-linked films containing SiC nanoparticles. The highest stiffness at the level of 82 GPa was found for films, which were both chemically cross-linked and modified by SiC nanoparticles introduction.

3.4. Cytotoxicity

The biological verification considered cytotoxicity of coatings modified by cross-linking or/and SiC nanoparticles has shown changes dependent on applied type of stabilization method (Fig. 9). Native (non cross-linked) Chi/CS films did not indicated cytotoxic effect in comparison with control culture. Moreover, cross-linking process did not change films influence on cellular viability. Films modified by 260 mM NHS/EDC indicated the same rate of death cells as native coatings and control. Significant increase of cytotoxicity was observed after SiC nanoparticles introduction into porous multilayer structure. Observed cytotoxic effect was significantly higher for SiC modified coatings which were cross-linked than those possess nanoparticles but not conducted to cross-linking process.

3.5. Coatings' settlement by endothelial cells

In this studies, either cross-linking or nanoparticles immobilization were applied to the polyelectrolyte multilayer properties control. Herein, we have compared influence of both stabilization methods and their combination on efficiency of Chi/CS films endothelialization (Fig. 10). Generally, cross-linked films indicated higher potential to settlement by endothelial cells than non-cross-linked multilayers probably due to their higher stiffness (the value nearest to control on polystyrene equal 5.02 cells number/cm^2 x 10^4. Moreover, in their native state, these films are highly hydrated such that they may impair cell adhesion [25, 26]. Nanoparticles introduction into non-cross-linked films increased endothelialization efficiency in comparison with non-cross-linked coatings without nanoparticles. However, cells density was significantly lower on non-cross-linked multilayers with SiC than on cross-linked coatings without nanoparticles. Furthermore, comparison of cross-linked coatings with nanoparticles and films which were conducted only to cross-linking has shown significantly lower cell number on films with SiC nanopaticles. Beyond of cells number determination, analysis of HUVECs included observations of their morphology. Cells condition was analyzed after DAPI and phalloidin staining. The changes in cell morphology were assessed based on comparison of cytoskeleton structure and nucleus localization in the cellular body. There was significant difference in cell shape and cytoskeleton architecture between investigated samples (Fig. 11). Typical shape for endothelial cells was observed only for cross-linked films without nanoparticles (similar to the control on the polystyrene – data not shown). On the rest of samples cells were rounded, with most of cytoplasma as thin layer condensed around relatively big nucleus. The exceptions were spindle-like cells which were formed long chains on the surface of non-crossed-linked coatings with introduced SiC nanoparticles. In order to quantify morphology similarities, the shape index (SI) was evaluated using image analysis. The SI is a dimensionless measure of cell roundness and is defined as:

$$SI=4\pi A/p^2 \quad (1)$$

where A is the area of a cell, and P is the length of cell perimeter. Thus, SI values range from zero for a straight line to unity for a perfect circle. Herein, the obtained value of SI differ between samples and was in range of 0.6±0.02 for endothelial cells on cross-linked films with proper cobblestone shape to 0.9±0.01 for cells on SiC modified coatings and 0.4 ±0.01 for SiC modified non-cross-linked samples with cells' chains. The SI for control cell culture on polystyrene was 0.6±0.01 (data not shown). Figure 12 demonstrates statistically significant differences between sample's circularity parameter.

4. Discussion

4.1. Topography and microstructure analysis

The microstructure of biomaterials plays a significant role in their mechanical properties and interactions with human cells and tissues. In this study internal structure of 48 bilayer Chi/CS films was modified by SiC nanoparticles. The effect of nanoparticles introduction was evaluated for native (non-cross-linked) and chemically cross-linked PEM films. It was found that size and distribution of SiC nanoparticles formed in PACVD process is independent on initial sample state. Topography changes observed in SEM images after nanoparticles introduction were similar for non-cross-linked and cross-linked films. However, initial condition of samples' roughness was different for non-cross-linked and cross-linked coatings. It was found that surface roughness was higher in case of non-cross-linked Chi/CS films. Contrary to observed phenomenon, it has been shown that roughness of other PEMs such as PLL/HA films increased after chemical cross-linking [27]. The TEM observations indicated no significant differences in nanoparticles size and zonal distribution between non-cross-linked and cross-linked Chi/CS coatings. Similar results were noticed for PLL/HA and PLL/ALG films [24]. The observed zonal nanoparticles arrangement was the effect of the penetration mechanism through the porous coating. Nanoparticles deposition process was based on plasma-activated nucleation from the gas phase. At first, formed nanoparticles have reached the polymer coating surface and have penetrated through the film's layers without incorporation. Then nanoparticles velocity decreased and the high SiC nanoparticles density zone was created. A small number of nanoparticles has penetrated through the film and formed the single SiC nanoparticles dispersion zone within lower coating layers. We suppose that charged nanoparticles interact with polymer films in varying degree depends on multilayer native or cross-linked state. The high surface energy makes them liable to undergo chemical reactions with the environment and self aggregation. Herein, PEMs internal structure differences were not observed based on SEM or TEM images, therefore in our opinion further FTIR investigations are desired to have a clear idea about nanoparticles – polyelectrolyte multilayer interactions. The another interesting issue which needs an experimental confirmation is the HMDSO derivatives role in cubic SiC nanoparticles formation within PEM films. It is well known that during the polymerization of hydrocarbon based gases in plasma, various steps of ionization, radical formation, dissociation and electronic excitation are triggered by inelastic collisions of energized electrons. This leads to fragmentation of gas molecules, leading in the case of HMDSO precursor to oxidized fragments (SiO, SiOx, SiOxCyHz, etc.) and hydrocarbons (CHx). Preferably, Si–C and C–H bonds are broken in the HMDSO molecule, due to lower binding energies of Si–C (4.5 eV) and C–H (3.6 eV) than the binding energy of Si–O (8.3 eV). While volatile derivatives such as COH_2, CO_2H_2, CO, CO_2, and H_2O are pumped off, fragments and simultaneously formed polymerizeable hydrocarbons (CH_4, C_2H_2) are able to react on the substrate surface. Silicon carbide nanoparticles were growing from such HMDSO derivatives. Usually, the reaction of C_2H_2 and molecules containing Si atoms, leading to an amorphous SiC nanoparticles formation. It has been shown that CH_4 molecules can trigger transition of 6H-SiC to cubic SiC nanoparticles. The described concept of cubic SiC nanoparticles introduction into PEMs should be verified by further investigations [28, 29, 30].

4.2. Nanoparticles dispersion numerical analysis

Numerical analysis allows for qualitative evaluation of the phenomena accompanying deformation process of Chi/CS porous material in the native state or after SiC nanoparticles incorporation. The material geometric models' permanent deformation was equal to Δl = 2800 nm. It has been found that ellipses (pores) located in the neighborhood of the indenter tip were closed in response to the applied load. During loading incensement the ellipses lying directly under indenter were being closed gradualy. The process have been continued until concerned all ellipses and the load was transferred to the substrate. After reaching the force F = 10 mN, unload process has occured at the intender. Ellipses were not permanently

deformed, therfore they have returned to the previous position. The most deformed ellipses were situated directly under the tip of the intender. It was found that proposed theoretical representation of PEMs could be applied to native Chi/CS films mechanical properties description. However, model application to films modified by SiC nanoparticles should be improved through the taking into account nanoparticles' inhomogeneous distribution within multilayer.

4.3. Experimental verification of coating's mechanical properties

The experimental verification has shown that results obtained from indentation tests are different than simulated mechanical properties probably due to inhomogeneous distribution of SiC nanoparticles. It was found that stiffness of Chi/CS films increased either after chemical cross-linking or SiC nanoparticles incorporation. Mechanical testing has shown that SiC nanoparticles allows for manufacturing PEMs with significantly higher stiffness than it is possible with application of NHS/EDC cross-linking chemistry. The Applied chemical cross-linking method modifid PEMs structure due to replacement of weak electrostatic interaction between polymer chains by strong covalent bonds. In case of SiC nanoparticles PEMs stiffness increased as a result of more interactions between polymer chains linked by nanoparticles as well as due to high Young modulus of silicon carbide material. PEMs structure modification leading to changes in mechanical properties is well described as a way of materials biocompatibility regulator. The NHS/EDC chemistry has been applied in order to control cellular adhesion and proliferation due to changes in PEMs rigidity [20, 31, 32, 33]. In our previous study, mechanical properties of PLL/HA films were established and described to find an optimal parameter for endothelial cells attachment and proliferation [27].

4.4. Cytotoxicity

The biocompatibility of individual polymers depends on different properties like molecular weight, charge density, type of cationic functionalities, structure, chemical sequence and conformational flexibility [16]. In general, the high charge of the synthetic polyelectrolytes (PEs) in solution influences the cell viability more than the low charge density of PEs from natural source. In this regard, Fischer et al. and Sgouras et al. found PEI and poly(L-lysine) very toxic for L929 mouse fibroblasts or hepato cellular carcinoma, respectively [34, 35]. Nolte at al. have shown similarly to our results that Chi and (HA/Chi) complexes indicate minimal toxicity at high concentrations [36]. Silva et al. have produced and characterized material combining chondroitin sulfate and fucoidan with chitosan for therapeutic purposes. Cytotoxicity tests resulted in non toxic effect of polymers on Caco-2 cell line. Viability of cell cultures wasnot affected after films chemical cross-linking by NHS/EDC reagents [37]. Cross-linker in adequate concentration results in irreversible linkage between layers responsible for coatings structure stabilization and swelling limitation. The potentially cytotoxic unbounded residues were precisely washed out from the coating, therefore cytotoxic effect was not noticed. Biocompatibility of NHS/EDC has been widely described in the literature [31]. The most important observation comes from this and recent study is that SiC nanoparticles cause a slight cytotoxic effect. The silicon carbide was considered in the literature mainly as a highly biocompatible material [38]. However, only a few toxicological data are available for these NPs. Barillet et al. presented global toxicological profile of SiC nanoparticles on A549 lung epithelial cells, using a battery of classical in vitro assays [39]. Allen et al. have investigated the effects of two forms of silicon carbide (alpha-SiC and beta-SiC) on macrophages, fibroblasts and bone cells in vitro and shown cytotoxicity of both forms at higher nanoparticles concentrations [40]. In this study we have shown that silicon carbide nanoparticles induced a slight but significant cell death. Higher necrotic effect of cross-linked films was observed probably due to lower contribution of polymer - nanoparticles interaction sides and higher particles release rate than in case of non-cross-linked films. Opposite results were found for PLL/HA and PLL/ALG films, where cytotoxicity of PEM-SiC nanoparticle composites was decreasing with application of higher concentrations of cross-linker [24]. This contrary could be explain by thinner HMDSO layer co-deposited during PACVD due to process parameters have been changed. In this case probably protective role of the HMDSO was less significant so only a number and character of nanoparticles-polyelectrolyte functional groups interactions was crucial for cytotoxicity. Moreover, we supposed that negatively charged nanoparticles are mostly stabilized by interaction with amine groups. In case of Chi/CS multilayers amine residues number is smaller than in case of PLL based multilayers. Then after chemical cross-linking by NHS/EDC less chemical groups are available for nanoparticles stabilization. For the films without SiC nanoparticles this results in lower Chi/CS films stiffness than in case of PLL/HA coatings after cross-linking by the same NHS/EDC reagents concentration. Similar tendency should be observed in case of films modified by SiC nanoparticles. It was shown that cross-linking decreased surface roughness of Chi/CS films without SiC nanoparticles contrary to effects observed for similar PLL/HA multilayers. Since we found that surface roughness after nanoparticles introduction did not depend on coating initial stage, we supposed that the same behavior could be noticed for films modified by nanoparticles. According to previous observations, changes in roughness and stiffness are important for adhesion of HMDSO thin layer co-deposited during PACVD process on the surface of PEM coating. We have observed better adhesive properties of HMDSO for the rougher and stiffer films. Therefore, in this studies observed cytotoxic effects could differ from those described for PLL/HA and PLL/ALG films due to lower HMDSO adhesion and higher human cells exposure on released SiC nanoparticles [24, 27].

4.5. Coatings' settlement by endothelial cells

Endothelial cells react mechano-sensitive to substrates and scaffolds applied for their culture [41]. It is stated that cells adhesion and proliferation depends mostly on PEMs properties such as stiffness, thickness, roughness and viscoelasticity [41, 42]. This leads to the fact that cells suffer from apoptosis when are seeded on soft coatings, especially in the case of natural polymers [16]. Moreover, it means that during the *in vitro* experiments, the cells do not necessarily die from cytotoxicity but from apoptosis caused of negligible adhesion to the underlying soft coating [26, 36]. Effects observed in this studies, indicated that SiC nanoparticles immobilization increased stiffness and changed other films properties which are crucial for endothelalization process. Nanoparticles introduction increased endthelialization efficiency in comparison to native (non-cross-linked) films. However, settlement of non-cross-linked films modified by SiC nanoparticles was lower than cross-linked films. Application of both stabilizers in the same time did not improve cellular adhesion and proliferation probably due to their additive effect on coating mechanical properties, which results in elevated stiffness above value optimal for HUVECs. Despite the apparent potential of CS, only a limited number of studies have been dedicated to the characterization and application of PEMs

assemblies containing CS [3, 26, 35]. Grohmann et al. have shown that cells density on pure CS films is extremely low [3]. The cells grown on (HA/Chi) or modified cross-linked (HA/Chi) indicated poor adhesion with a rounded cell shape [43, 44]. Only few studies have been dedicated to the influence of using multiple polysaccharides for film construction on the resulting secondary structure of the assembly [45]. However it was shown that well organized structure like β-sheets could be responsible for cellular better adhesion and proliferation than random coils or α-helix structures. It seems to be essential to describe in the future research if nanoparticles are influential for polysaccharides structure organization and then changes in mechanical properties of films. Equally interesting will be evaluation how SiC nanoparticles introduction due to surface roughness and wettability changes impact on HUVECs response.

5. Conclusions

Comparison of the stabilization method including chemical cross-linking and SiC nanoparticles introduction into multilayer polyelectrolyte films has shown that both of stabilizers could be useful for biomedical applications. However, SiC nanoparticles application could be limited by slightly lower endothelialization efficiency and risk of cytotoxicity due to their release from coatings. Following the theoretical analysis SiC nanoparticles should be uniformly distributed in the multilayer. Experimental verification did not confirm the simulation thesis. HRTEM images revealed formation of three zones within polyelectrolyte multilayer instead of homogenous particles dispersion. Moreover, experimental verification has shown that simulated mechanical properties are different than results obtained from indentation tests. Mechanical testing has shown that SiC nanoparticles incorporation allows for manufacturing PEMs with significantly higher stiffness than it is possible with application of NHS/EDC cross-linking chemistry. The performed studies allowed coming to correlations between the Chi/CS film structure, its mechanical properties and the bioeffects in response to stabilization by chemical cross-linking or SiC nanoparticles. Future investigations should be concentrated on PACVD method improvement in order to obtain mono-dispersive, non-aggregated nanoparticles distribution in films. Character of nanoparticles interactions with multilayers and their influence on polysaccharides conformation needs to be determined in further research. Fascinating could be correlation of this issue with changes in mechanical and surface properties of biocomposites.

Acknowledgements

The research was financially supported by the European Union under the European Social Found within Project No. POKL.04.01.00-00-004/10 and Project No. 2011/03/D/ST8/04103 "Self-assembling, biomimetic porous scaffolds in terms of inhibiting the activation of the coagulation system" of the Polish National Center of Science.

Notes and references

[a] Institute of Metallurgy and Materials Science, Polish Academy of Sciences, 25 Reymonta Street, 30-059 Krakow, Poland.
[b] Joanneum Research Forschungsges mbH, Institute of Surface Technologies and Photonics, Functional Surfaces, Leobner Strasse 94, A-8712 Niklasdorf, Austria.
[c] Laboratoire des Matériaux et du Génie Physique Grenoble Institute of Technology, Grenoble, France
[d] Foundation for Cardiac Surgery Development, Wolnosci Street 345a, 41-800 Zabrze, Poland

1. J. Fu, J. Ji, W. Yuan, J. Shen, *Biomaterials*, 2005, **26**(33), 6684– 6692.
2. K. Abdelkebir, F. Gaudie`re, S. Morin-Grognet, G. Coquerel, H. Atmani, B. Labat, G. Ladam, *Langmuir*, 2011, **27**(23), 14370–14379.
3. S. Grohmann, H. Rothe, K. Liefeith, *Biointerphase*, 2012; **7**, 62.
4. D. Archana, L. Upadhyay, R. P. Tewari, J. Dutte, Y. B. Huang, P. K. Dutta, *Indian Journal of Biotechnology*, 2013, **12**, 475:482.
5. M. L. Macdonald, N. M. Rodriguez, N. J. Shah, P. T. Hammond, *Biomacromolecules*, 2010, **11**(8), 2053–2059.
6. L. Ma, J. Zhou, C. Gao, J. Shen, *J Biomed Mater Res Part B: Appl Biomater,* 2007, **83B**, 285–292.
7. G. A. Hudalla, W. L. Murphy, *Adv Funct Mater,* 2011, **21**(10), 1754–1768.
8. M. K. Gheith, V. A. Sinani, J. P. Wicksted, R. L. Matts, N. A. Kotov. *Adv Mater,* 2005, **17**(22), 2663−2667.
9. C. Jiang, V. Tsukruk, *Adv Mater,* 2006, **18**, 829−840.
10. V. Gribova, R. Auzely-Velty, C. Picart, *Chemistry of Materials*, 2012, **24**, 854-869.
11. L. Shen, L. Rapenne, P. Chaudouet, J. Ji, C. Picart, *J Colloid Interface Sci*, 2012, **388**, 56–66.
12. J. Fu, J. Ji, D. Fan, J. Shen, *J Biomed Mater Res,* 2006, **79A**, 665–674.
13. W. Y. Yuan, J. H. Fu, K. Su, J. Ji, *Colloids Surf. B Biointerfaces*, 2010, **76**(2), 549–555.
14. A. Agarwal, T. L. Weis, M. J. Schurr, N. G. Faith, C. J. Czuprynski, J. F. McAnulty, C. J. Murphy, N. L. Abbott, *Biomaterials*, 2010, **31**(4), 680–690.
15. Z. Tang, Y. Wang, P. Podsiadlo, N. Kotov, *Adv Mater*, 2006, **18**(24), 3203-3224.
16. C. Picart, *Curr Med Chem*, 2008, **15**(7), 685–697.
17. H. Zhao, L. Shi, Z. Li, C. Tang, *Phys E,* 2009, **41**, 753-756.
18. R. Ghavamia, A. Salimi, A. Navaee, *Biosens Bioelectron*, 2011, **26**(9), 3864–3869.
19. S. Miserere, S. Ledru, N. Ruille, S. Griveau, M. Boujtita, F. Bedioui, *Electrochem Commun*, 2006, **8**, 238–244.
20. L. Richert, F. Boulmedais, P. Lavalle, J. Mutterer, E. Ferreux, G. Decher, P. Schaaf, J. Voegel, C. Picart, *Biomacromolecules*, 2004, **5**(2), 284−294.
21. J. M. Lackner, W. Waldhauser, R. Major, L. Major, P. Hartmann, *Surf Coat Technol*, 2013, **215**, 192–198.
22. L. Major, W. Tirry, G. Van Tendeloo, *Surf Coat Technol*, 2008, **202**(24), 6075-6080.

23. ISO 10993-5 2009: "Biological evaluation of medical device – Part 5: "Tests for in vitro cytotoxicity".
24. A. Mzyk, R. Major, J. M. Lackner, F. Bruckert, B. Major, *RSC Adv*, 2014, **4**, 31948-31954.
25. K. Abdelkhebir, F. Gaudière, S. Morin-Grognet, G. Coquerel, B. Labat, H. Atmani, G. Ladam, *Soft Matter*, 2011, **7**, 9197-9205.
26. F. Gaudière, I. Masson, S. Morin-Grognet, O. Thoumire, J. P. Vannier, H. Atmani, G. Ladam, B. Labat, *Soft Matter*, 2012, **8**, 8327-8337.
27. A. Mzyk, R. Major, M. Kot, J. Gostek, P. Wilczek and B. Major, *Archives of Civil and Mechanical Engineering*, 2014, **14**(2), 262–268.
28. J. M. Lackner, M. Wiesinger, R. Kaindl, W. Waldhauser, D. Heim, P., Hartmann, *Plasma Chem Plasma Process*, 2014, **34**, 259–269.
29. D. Siye, Y. Guanchao, Z. Xiaodong, Z. Haiyang, *Plasma Sci. Technol.*, 2009, **11**, 159.
30. Y. Wang, J. Zhang, X. Shen, *Mater Chem Phys*, 2006, **96**, 498–505.
31.29. C. P. Vazquez, T. Boudou, V. Dulong, C. Nicolas, C. Picart, K. Glinel, *Langmuir*, 2009, **25**(6), 3556–3563.
32. A. Schneider, G. Francius, R. Obeid, P. Schwinté, B. Frisch, P. Schaaf, J. C. Voegel, B. Senger, C. Picart, *Langmuir*, 2006, **22**, 1193–1200.
33. C. Boura, P. Menu, E. Payan, C. Picart, J. C. Voegel, S. Muller, J. F. Stoltz, *Biomaterials*, 2003, **24**, 3521–3530.
34. D. Fischer, Y. Li, B. Ahlemeyer, J. Krieglstein, T. Kissel, *Biomaterials*, 2003, **24**(7), 1121–1131.
35. D. D. R. Sgouras, R. Duncan, *J Mater Sci*: *Mater Med,* 1990, **1**, 61–68.
36. A. Nolte, S. Hossfeld, B. Schroeppel, A. Mueller, D. Stoll, T. Walker, H. P. Wendel, R. Krastev, *Journal of Biomaterials Applications*, 2012, **28**(1), 84–99.
37. L. C. da Silva, T. Garcia, M. Mori, G. Sandri, M. C. Bonferoni, P. V. Finotelli, L. P. Cinelli, C. Caramella, L. M. Cabral, *International Journal of Nanomedicine*, 2012, **7**, 2975–2986.
38. J. Pourchez, V. Forest, N. Boumahdi, D. Boudard, M. Tomatis, B. Fubini, N. Herlin-Boime, Y. Leconte, B. Guilhot, M. Cottier, P. Grosseau, *J Nanopart Res*, 2012, **14**(10), 1143-1147.
39. S. Barillet, M. L. Jugan, M. Laye, Y. Leconte, N. Herlin-Boime, C. Reynaud, M. Carriere, *Toxicol Lett*, 2010, **198**(3), 324–330.
40. M. Allen, R. Butter, L. Chandra, A. Lettington, N. Rushton, *Biomed Mater Eng*, 1995, **5**(3), 151–159.
41. Y. Shen, G. Wang, X. Huang, *J R Soc Interface*, 2012, **9**(67), 313-27.
42. R. R. Costa, C. A. Custodio, F. J. Arias, *Small*, 2011, **7**(18), 2640-2649.
43. C. A. Holmes, M. Tabrizian, *J Biomed Mater Res A*, 2012, **100**(2), 518-26.
44. A. Schneider, L. Richert, G. Francius, J. V. Voegel, C. Picart, *Biomed Mater*, 2007, **2**(1), 45-51.
45. A. Forget, J. Christensen, S. Lüdeke, E. Kohler, S. Tobias, M. Matloubi, R. Thomann, V. P. Shastri, *PNAS*, 2013, **110**(32), 12887–12892.

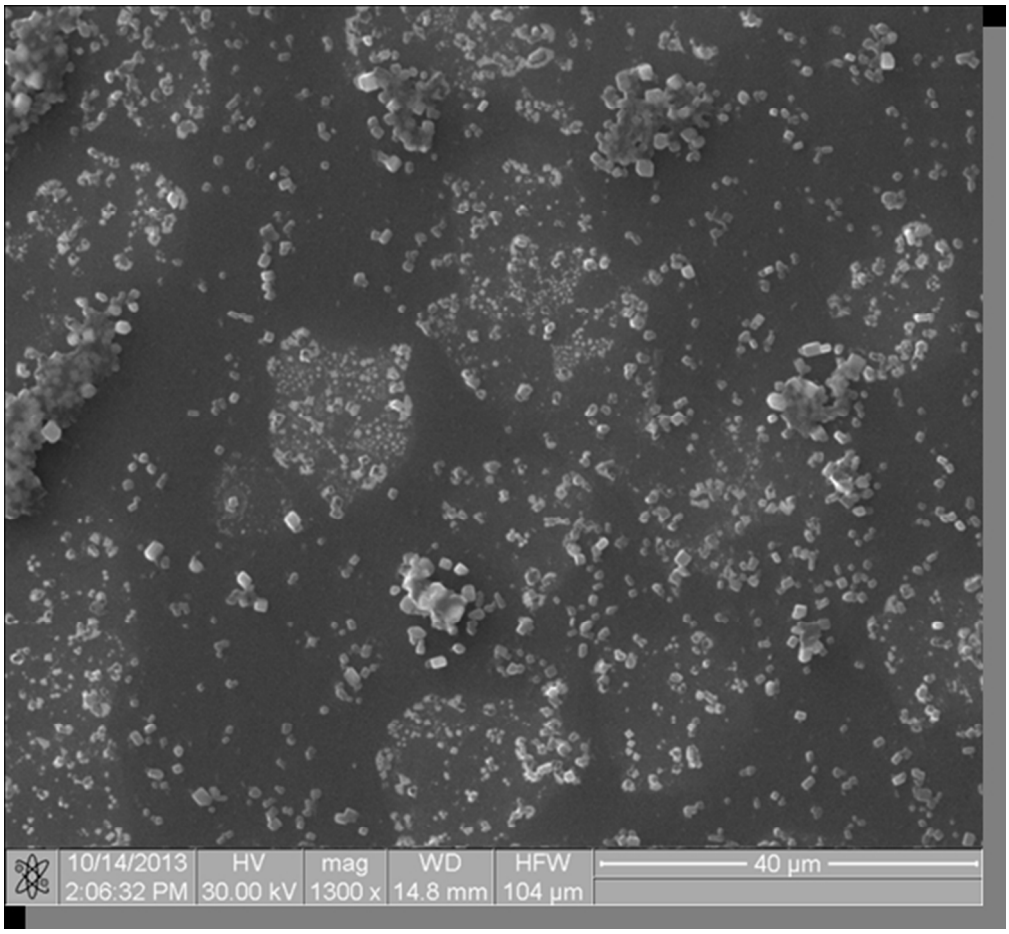

Fig.1 The SEM image of SiC nanoparticles aggregate-like structure formation nd distribution within 48 bilayer Chi/CS films cross-linked by 100 mM NHS/260 mM EDC reagents.
100x92mm (150 x 150 DPI)

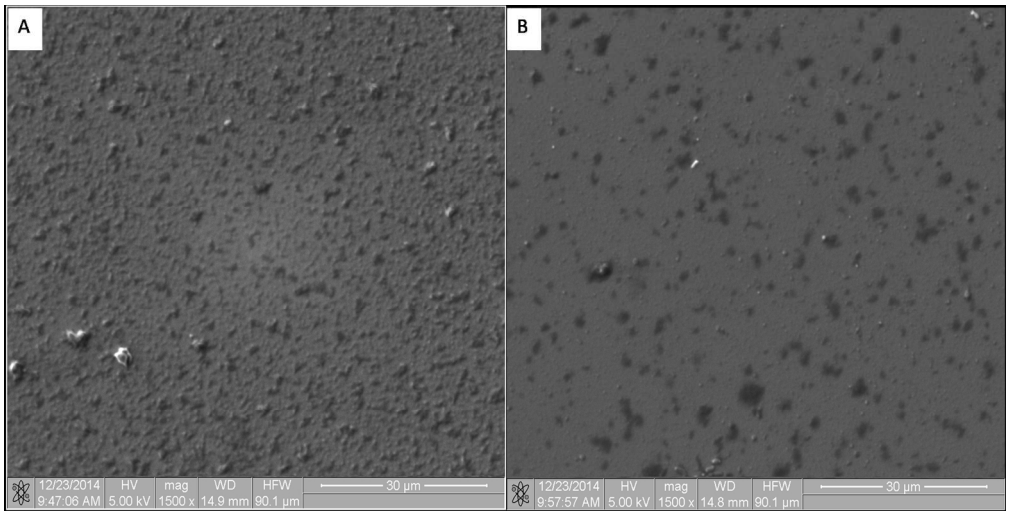

Fig.2 The SEM surface topography of A) non-cross-linked and B) cross-linked 48 bilayer Chi/CS films.
304x153mm (150 x 150 DPI)

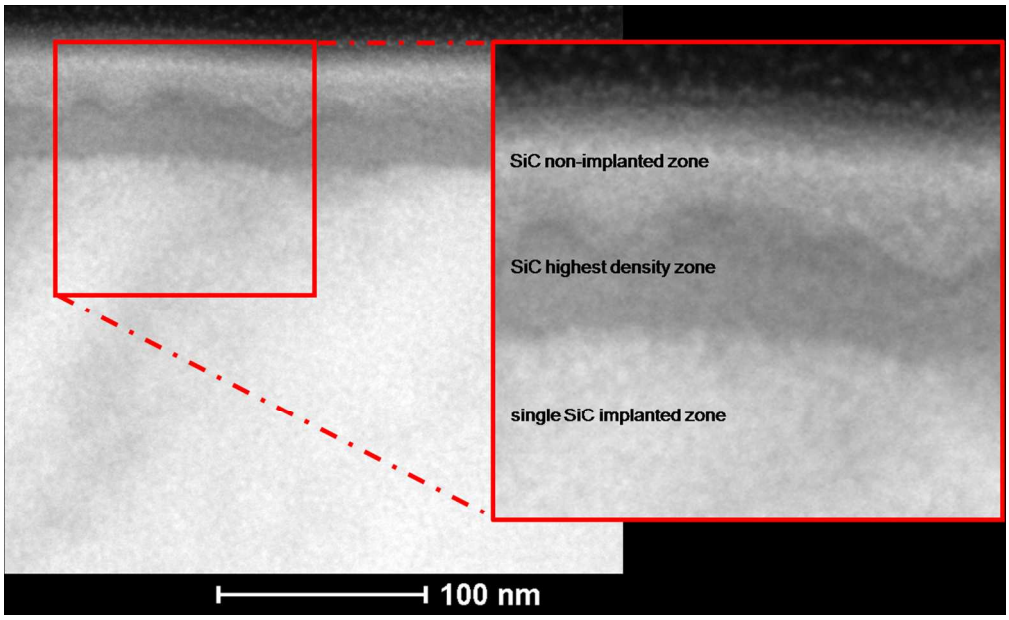

Fig.3 The TEM cross section image of SiC nanoparticles localization within 48 bilayer Chi/CS chemically cross-linked coating.
227x138mm (150 x 150 DPI)

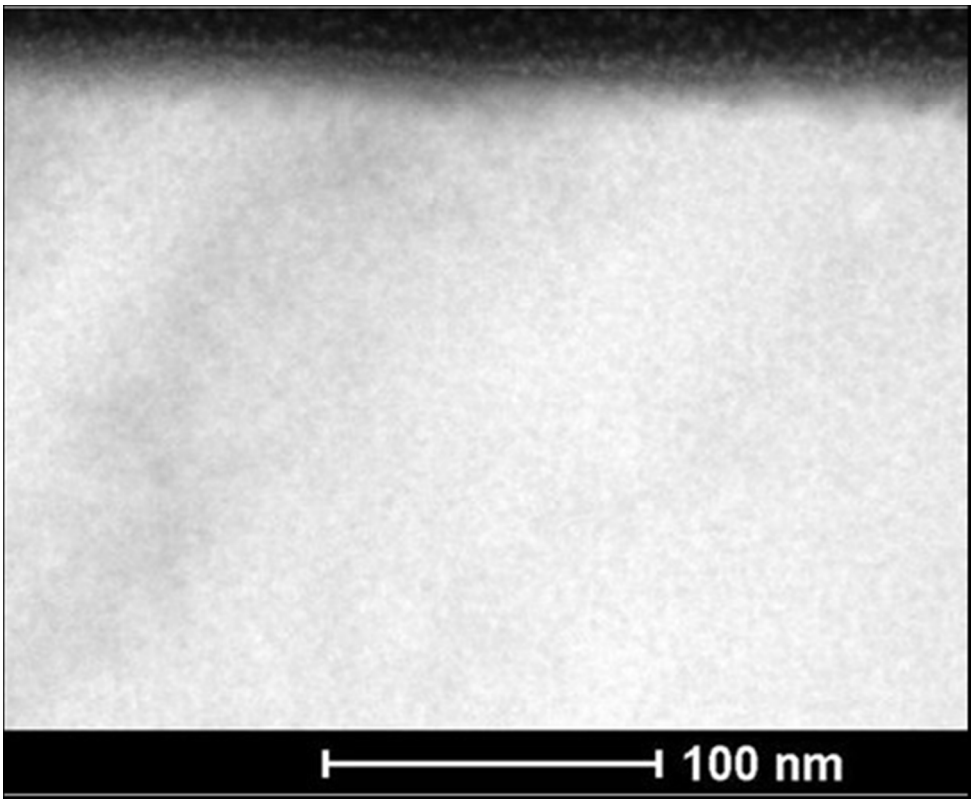

Fig.4 The TEM cross section image of 48 bilayer Chi/CS chemically cross-linked coating amorphous structure.
183x150mm (67 x 67 DPI)

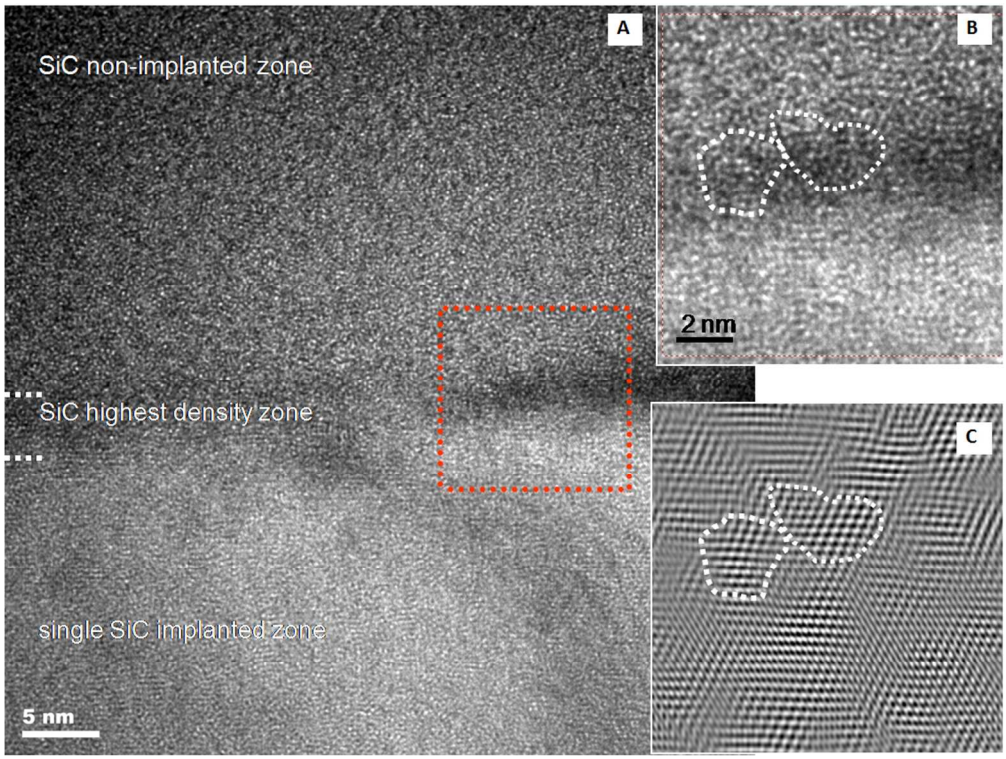

Fig.5 HRTEM analysis of the silicon carbide nanoparticles introduction into porous polymer coating A) zonal distribution of SiC nanoparticles within 48 bilayer Chi/CS films; B) unfiltered image and C) filtered image for identification of the SiC cubic structure.
298x224mm (96 x 96 DPI)

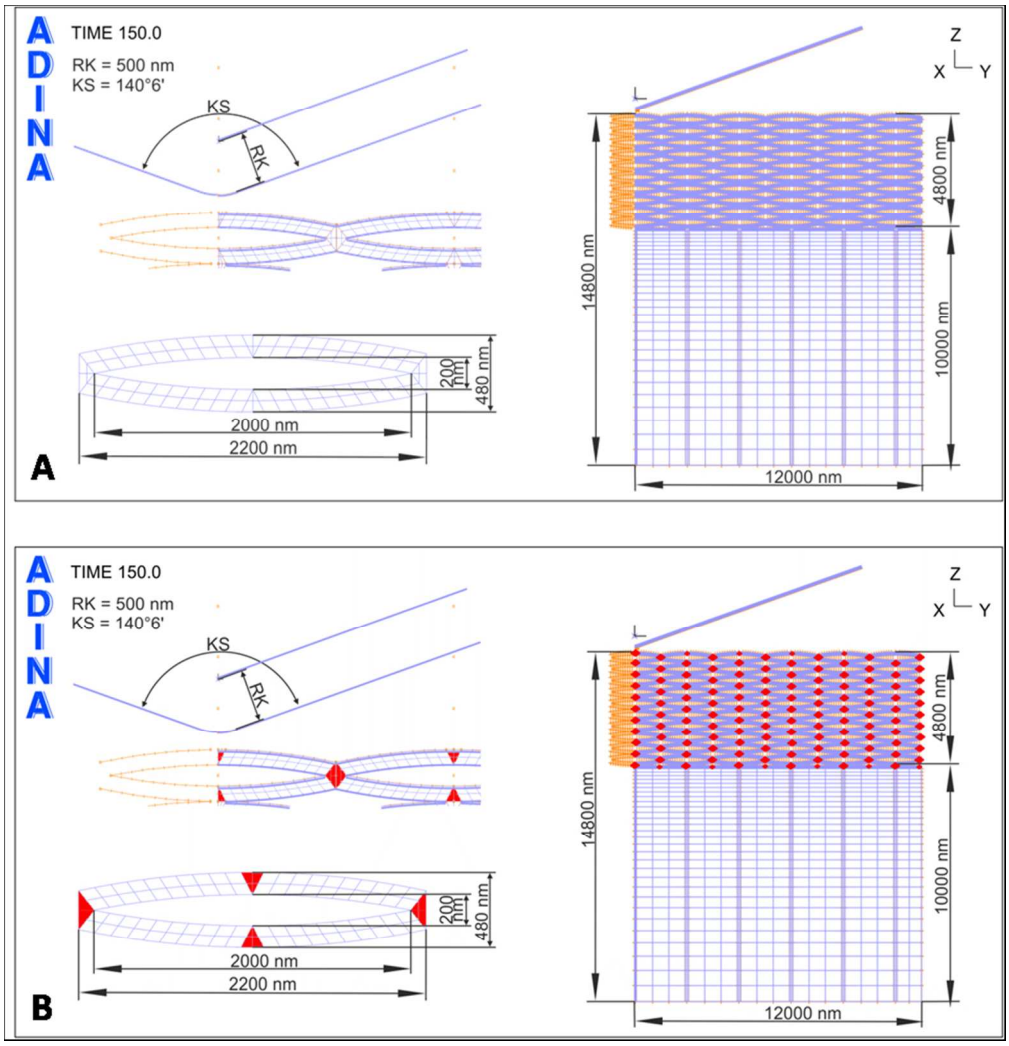

Fig.6 Geometric model of A) glass substrate and Chi/CS polyelectrolyte film; B) glass substrate and Chi/CS polyelectrolyte film stabilized by SiC nanoparticles.
165x170mm (147 x 147 DPI)

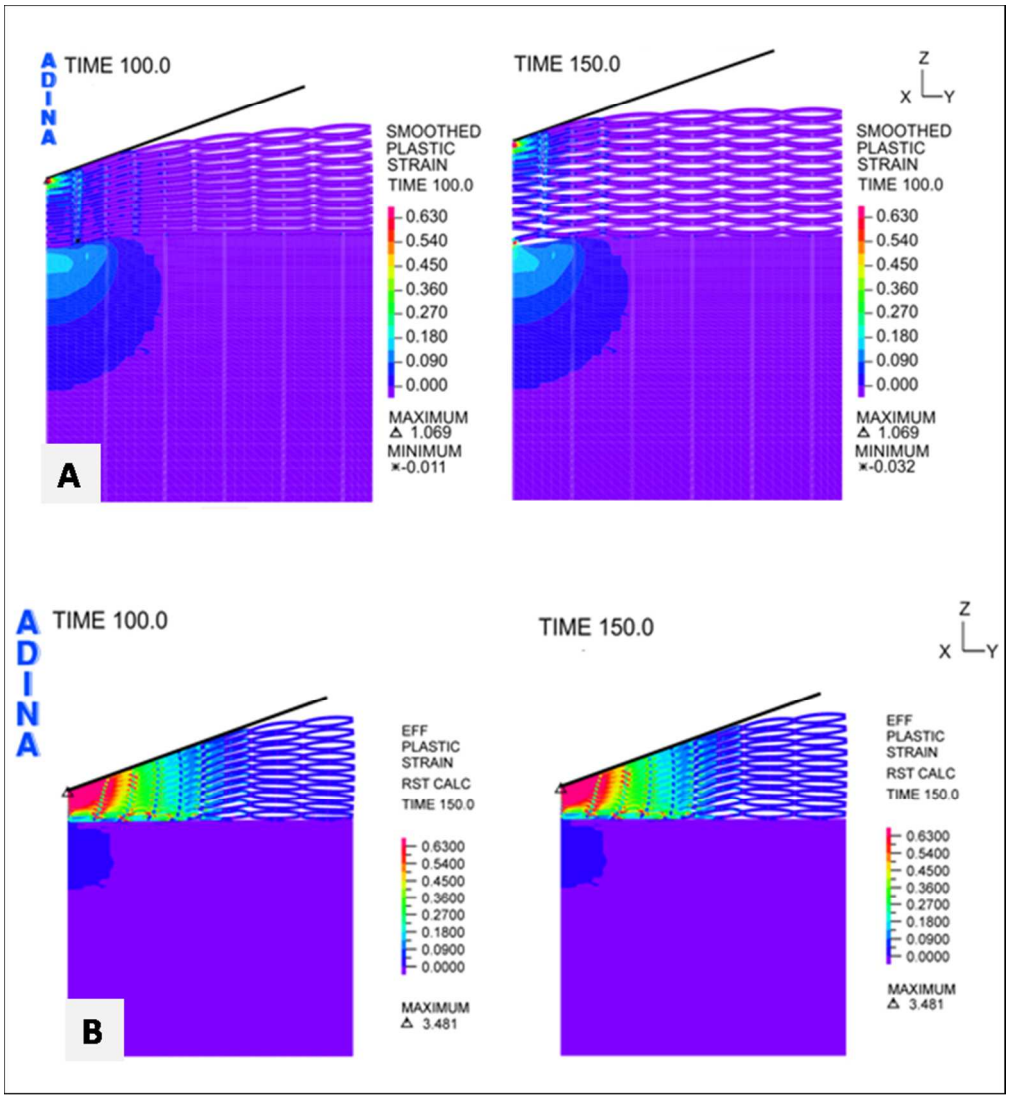

Fig.7 Distribution of plastic deformation at the time of loading and unloading A) glass substrate and Chi/CS polyelectrolyte film; B) glass substrate and Chi/CS polyelectrolyte film stabilized by SiC nanoparticles.
167x182mm (150 x 150 DPI)

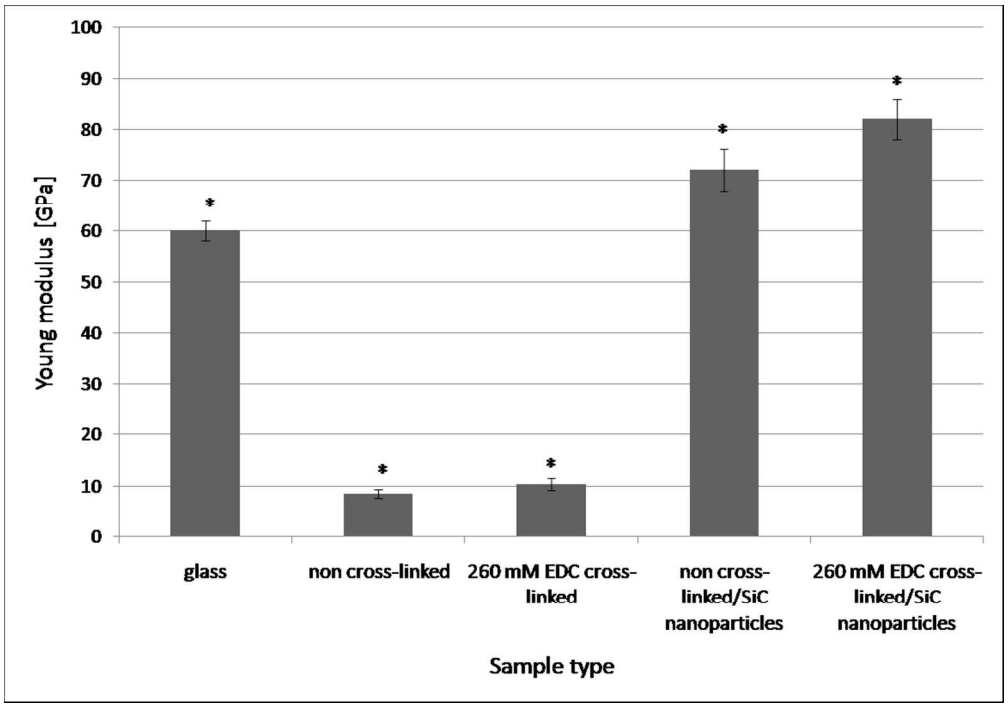

Fig.8 The mechanical properties (Young modulus) comparison of glass substrate; native (non stabilized) 48 bilayer Chi/CS films and the same coating type stabilized by SiC nanoparticles or NHS/EDC cross-linking process. Data represent mean ±SD; n=10; *P < 0.05 vs. sample non-cross-linked without NPs.
197x137mm (150 x 150 DPI)

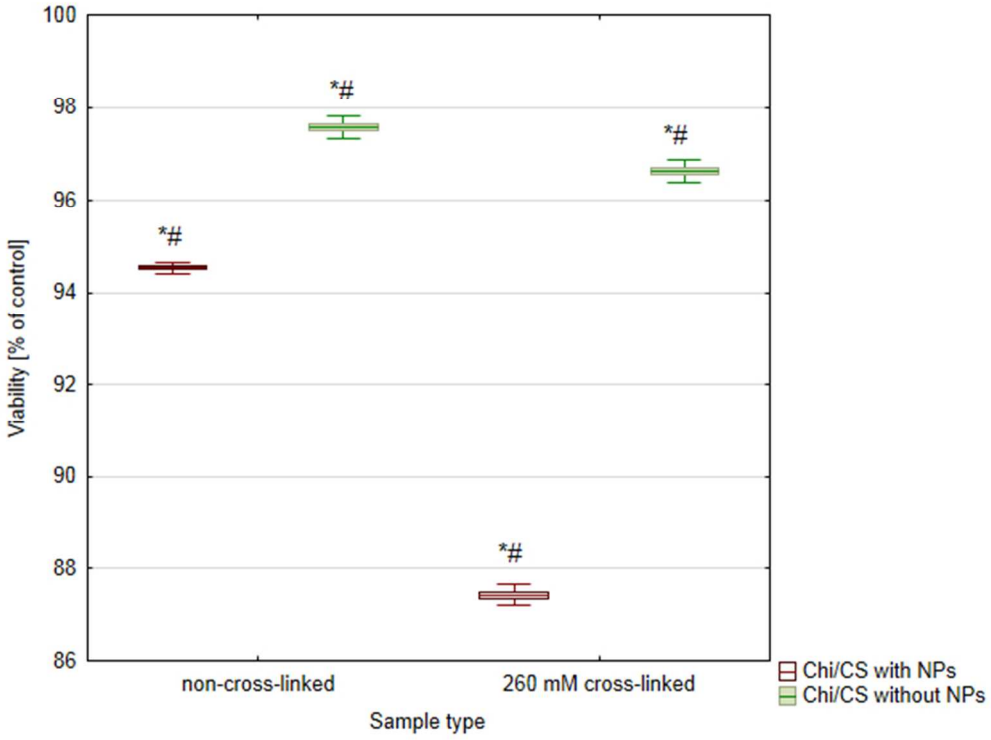

Fig.9 Cytotoxicity analysis of 48 bilayer Chi/CS films stabilized by SiC nanoparticles or NHS/EDC cross-linking process. Data represent mean ±SD; n=3; *P < 0.05 vs. sample non-cross-linked without NPs, #P < 0.05 vs. sample non-cross-linked with NPs.
165x123mm (96 x 96 DPI)

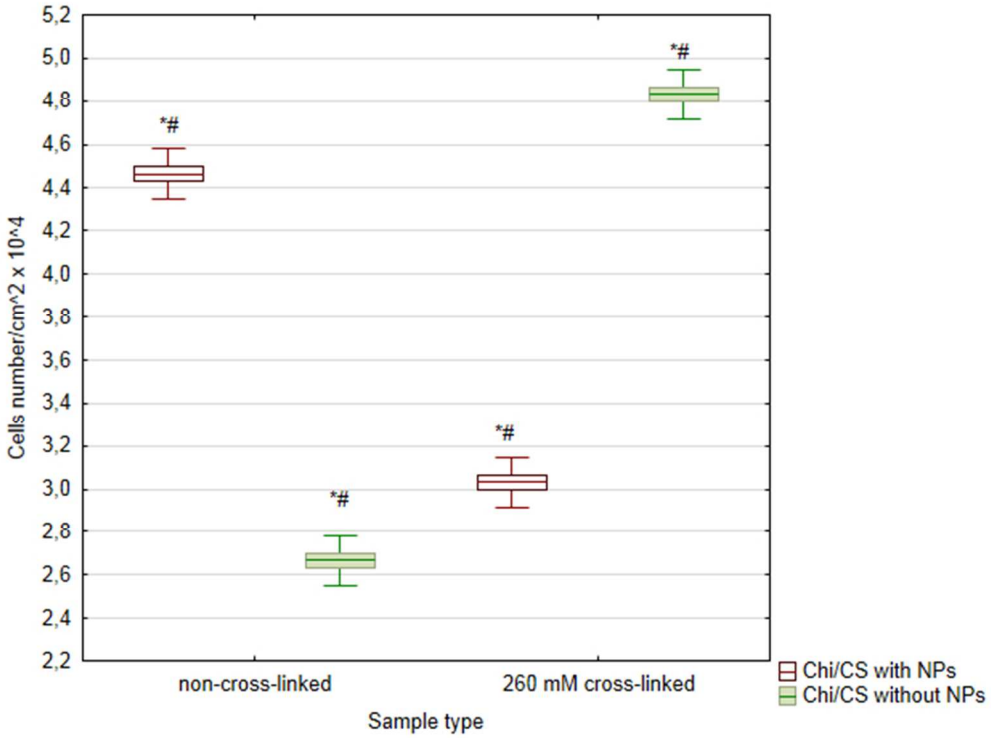

Fig.10 The average number of HUVECs after 4 days of growth on 48 bilayer Chi/CS films stabilized by NHS/EDC chemical cross-linking or SiC nanoparticles introduction. Data represent mean ±SD; n=3; *P < 0.05 vs. sample non-cross-linked without NPs, #P < 0.05 vs. sample non-cross-linked with NPs.
165x123mm (96 x 96 DPI)

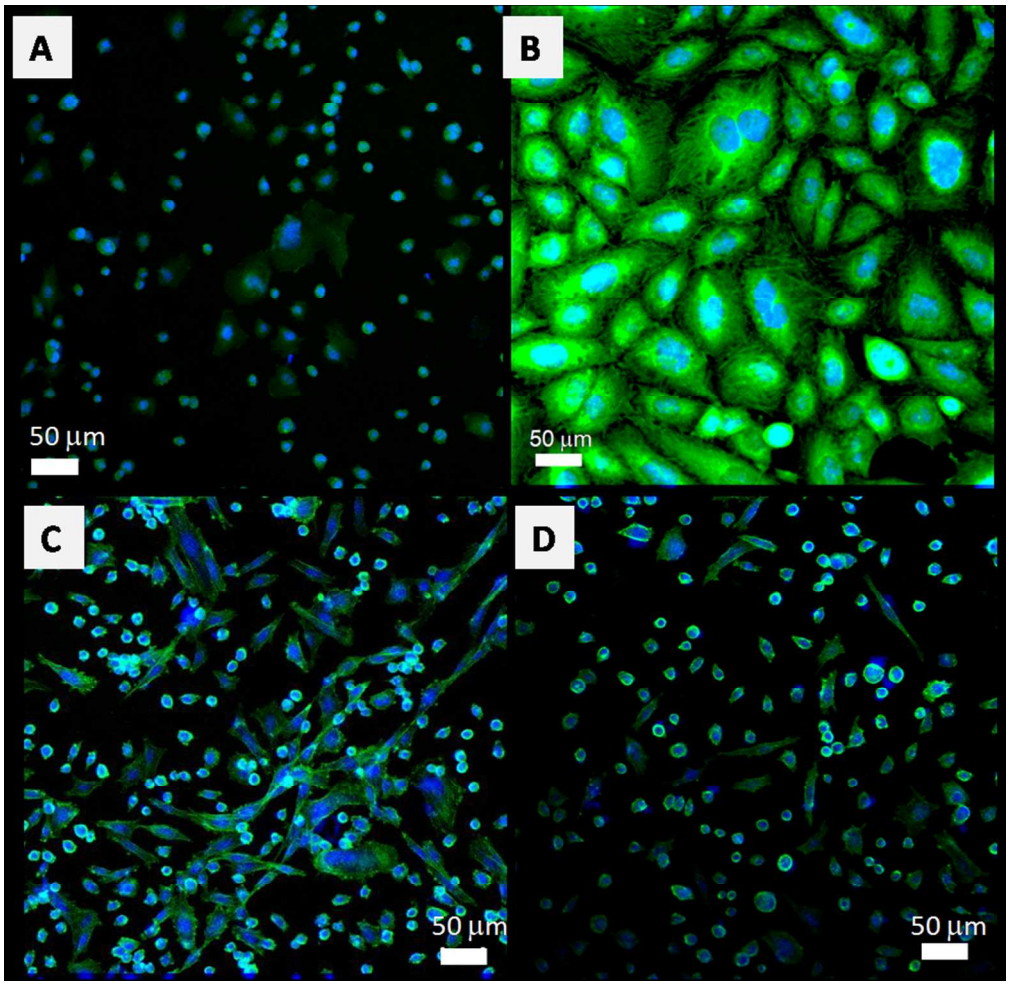

Fig.11 Morphology of HUVECs after 4 days of growth. Cells were seeded on 48 bilayer Chi/CS films A) non-cross-linked; B) cross-linked by NHS/EDC; C) non-cross-linked and stabilized by SiC nanoparticles; D) cross-linked by NHS/EDC and stabilized by SiC naoparticles.
166x161mm (150 x 150 DPI)

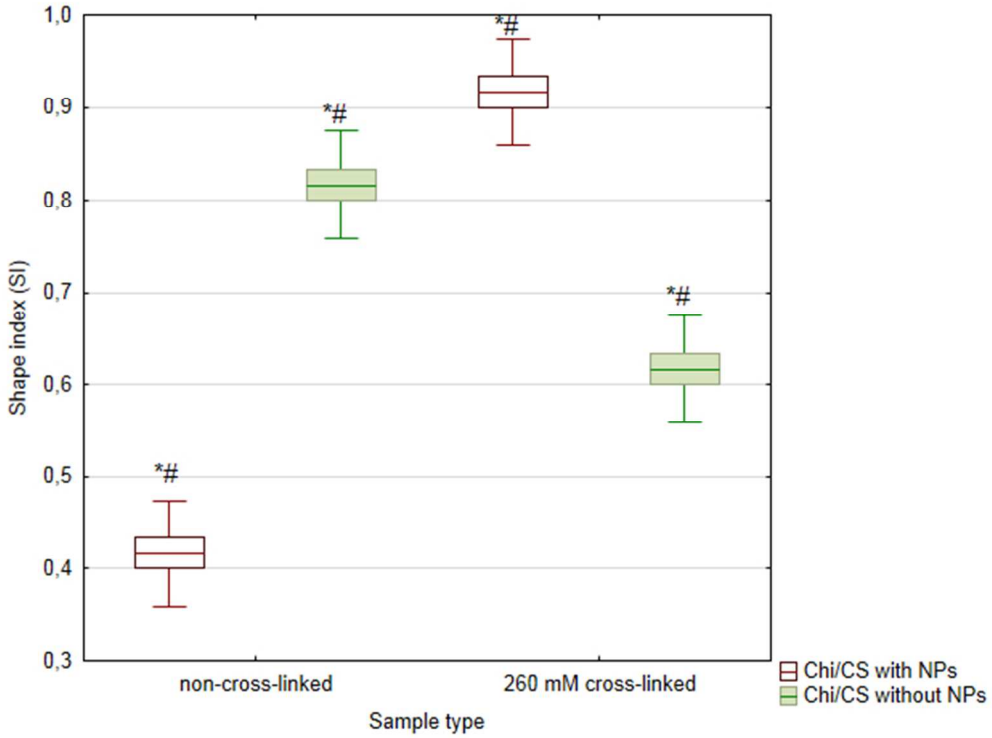

Fig.12 Sample's circularity parameter (SI) of HUVECs after 4 days of growth on 48 bilayer Chi/CS films stabilized by NHS/EDC chemical cross-linking or SiC nanoparticles introduction. Data represent mean ±SD; n=3; *P < 0.05 vs. sample non-cross-linked without NPs, #P < 0.05 vs. sample non-cross-linked with NPs.
165x123mm (96 x 96 DPI)

Table 1 Prepared 48 bilayer Chi/CS coating variants.

Sample number	Number of bilayers	Polymer type	Cross-linking	Nanoparticles introduction
1	48 bilayers	Chitosan/ chondroitin sulfate	non	non
2			non	SiC nanoparticles
3			100 mM NHS/ 260 mM EDC	non
4			100 mM NHS/260 mM EDC	SiC nanoparticles

Table 2 Indenter load in time.

Time, s	**0**	**20**	**40**	**60**	**80**	**100**	**120**	**140**	**150**
Force, mN	**0**	**0,068**	**0,257**	**0,52**	**0,788**	**1**	**0,52**	**0,13**	**0**

Table 3 The 48 bilayer Chi/CS coating with or without SiC nanoparticles and the glass substrate mechanical properties introduced into the model.

Material	Young modulus E, GPa	Poisson coefficient ν	The yield strength $R_{p0.2}$, MPa
Polymer coating	0,1	0,3	160
Substrate (glass)	70	0,3	800
SiC nanoparticles	170	0,3	6000

List of figure and table captions

Fig. 1 The SEM image of SiC nanoparticles aggregate-like structure formation nd distribution within 48 bilayer Chi/CS films cross-linked by 100 mM NHS/260 mM EDC reagents.

Fig. 2 The SEM surface topography of A) non-cross-linked and B) cross-linked 48 bilayer Chi/CS films.

Fig. 3 The TEM cross section image of SiC nanoparticles localization within 48 bilayer Chi/CS chemically cross-linked coating.

Fig. 4 The TEM cross section image of 48 bilayer Chi/CS chemically cross-linked coating amorphous structure.

Fig. 5 HRTEM analysis of the silicon carbide nanoparticles introduction into porous polymer coating A) zonal distribution of SiC nanoparticles within 48 bilayer Chi/CS films; B) unfiltered image and C) filtered image for identification of the SiC cubic structure.

Fig. 6 Geometric model of A) glass substrate and Chi/CS polyelectrolyte film; B) glass substrate and Chi/CS polyelectrolyte film stabilized by SiC nanoparticles.

Fig. 7 Distribution of plastic deformation at the time of loading and unloading A) glass substrate and Chi/CS polyelectrolyte film; B) glass substrate and Chi/CS polyelectrolyte film stabilized by SiC nanoparticles.

Fig. 8 The mechanical properties (Young modulus) comparison of glass substrate; native (non stabilized) 48 bilayer Chi/CS films and the same coating type stabilized by SiC nanoparticles or NHS/EDC cross-linking process. Data represent mean ±SD; n=10; *P < 0.05 vs. sample non-cross-linked without NPs.

Fig. 9 Cytotoxicity analysis of 48 bilayer Chi/CS films stabilized by SiC nanoparticles or NHS/EDC cross-linking process. Data represent mean ±SD; n=3; *P < 0.05 vs. sample non-cross-linked without NPs, #P < 0.05 vs. sample non-cross-linked with NPs.

Fig. 10 The average number of HUVECs after 4 days of growth on 48 bilayer Chi/CS films stabilized by NHS/EDC chemical cross-linking or SiC nanoparticles introduction. Data represent mean ±SD; n=3; *P < 0.05 vs. sample non-cross-linked without NPs, #P < 0.05 vs. sample non-cross-linked with NPs.

Fig. 11 Morphology of HUVECs after 4 days of growth. Cells were seeded on 48 bilayer Chi/CS films A) non-cross-linked; B) cross-linked by NHS/EDC; C) non-cross-linked and stabilized by SiC nanoparticles; D) cross-linked by NHS/EDC and stabilized by SiC naoparticles.

Fig. 12 Sample's circularity parameter (SI) of HUVECs after 4 days of growth on 48 bilayer Chi/CS films stabilized by NHS/EDC chemical cross-linking or SiC nanoparticles introduction. Data represent mean ±SD; n=3; *P < 0.05 vs. sample non-cross-linked without NPs, #P < 0.05 vs. sample non-cross-linked with NPs.

Table 1 Prepared 48 bilayer Chi/CS coating variants.

Table 2 Indenter load in time.

Table 3 The 48 bilayer Chi/CS coating with or without SiC nanoparticles and the glass substrate mechanical properties introduced into the model.